Loosening Quantum Confinement: Observation of Real Conductivity Caused by Hole Polarons in Semiconductor Nanocrystals Smaller than the Bohr Radius

Ronald Ulbricht,[†,‡] Joep J. H. Pijpers,[†,‡] Esther Groeneveld,[§] Rolf Koole,[§] Celso de Mello Donega,[§] Daniel Vanmaekelbergh,[§] Christophe Delerue,[∥] Guy Allan,[∥] and Mischa Bonn*[,†,‡]

[†]FOM Institute AMOLF, Amsterdam, Science Park 104, 1098 XG Amsterdam, Netherlands

[‡]Max Planck Institute for Polymer Research, Ackermannweg 10, 55128 Mainz, Germany

[§]Utrecht University, P.O. Box 80000, 3508 TA Utrecht, Netherlands

[∥]IEMN - Department ISEN, 41 Boulevard Vauban, 59046 Lille Cedex, France

Supporting Information

ABSTRACT: We report on the gradual evolution of the conductivity of spherical CdTe nanocrystals of increasing size from the regime of strong quantum confinement with truly discrete energy levels to the regime of weak confinement with closely spaced hole states. We use the high-frequency (terahertz) real and imaginary conductivities of optically injected carriers in the nanocrystals to report on the degree of quantum confinement. For the smaller CdTe nanocrystals (3 nm < radius < 5 nm), the complex terahertz conductivity is purely imaginary. For nanocrystals with radii exceeding 5 nm, we observe the onset of real conductivity, which is attributed to the increasingly smaller separation between the hole states. Remarkably, this onset occurs for a nanocrystal radius significantly smaller than the bulk exciton Bohr radius $a_B \sim 7$ nm and cannot be explained by purely electronic transitions between hole states, as evidenced by tight-binding calculations. The real-valued conductivity observed in the larger nanocrystals can be explained by the emergence of mixed carrier-phonon, that is, polaron, states due to hole transitions that become resonant with, and couple strongly to, optical phonon modes for larger QDs. These polaron states possess larger oscillator strengths and broader absorption, and thereby give rise to enhanced real conductivity within the nanocrystals despite the confinement.

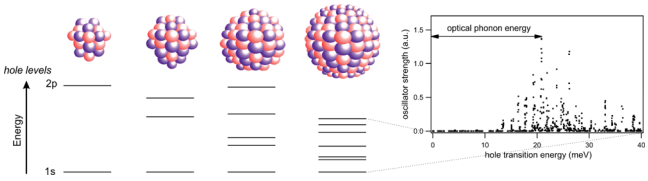

KEYWORDS: *Quantum dots, nanocrystals, polaron, quantum confinement, terahertz spectroscopy, intraband absorption, conductivity*

Downsizing semiconductor structures into the nanometer scale is an important trend in electronic research and manufacturing, not only for the resulting increase in performance and compactness of electronic devices. Electronic quantum confinement occurring in materials possessing dimensions smaller than the charge carrier wave function provides a unique means for tailoring electronic properties. Among zero-dimensional semiconductor nanostructures, that is, quantum dots, colloidal nanocrystals have proven to be particularly useful in optoelectronic devices such as displays and solar cells, largely due to the tunability of the bandgap by size[1] in conjunction with simple solution processing and ample control over surface functionality.

The degree of electronic confinement is commonly determined by the ratio between the nanocrystal radius R and the bulk exciton Bohr radius a_B, and materials are classified accordingly into the strong ($R/a_B < 1$), intermediate ($R/a_B \sim 1$), or weak ($R/a_B \gg 1$) quantum confinement regime.[2] Colloidal semiconductor nanocrystals are typically manufactured to be in the strong confinement regime. Such nanoparticles are characterized by the occurrence of discrete, "atom-like" electronic states as a result of the spatial quantum confinement of electron and hole wave functions. The electronic properties of small nanoparticles are fundamentally different from their larger-sized (or bulk) counterparts, where electronic states form continuous bands. Electronic conduction in the classical sense is absent in these nanoparticles due to the lack of closely spaced electronic levels into which carriers can scatter and consequently gain a directional net momentum when an electric field is applied. Indeed, the complex conductivity of charge carriers in strongly confining quantum dots has been shown to have a finite imaginary, but zero real-valued component.[3] The imaginary conductivity arises from the polarizability of electrons and holes within the nanocrystals, since the extended wave functions are highly polarizable under the influence of external electric fields.[4]

A relevant and fundamental question arises in the transition region, where the nanocrystal size starts to exceed the exciton Bohr radius, that is, in the intermediate regime between the limits of weak and strong quantum confinement. Theoretical and experimental efforts have shown that the electronic

structure remains altered as compared to the bulk case, even for nanocrystal sizes well above the exciton Bohr radius.[5] However, real conductivity at terahertz (THz) frequencies has been reported for nanocrystals of sizes around the exciton Bohr radius, which was attributed to freely moving charges in continuous electronic states.[6] This seeming discrepancy raises an interesting question: at what size and through which mechanism does real conductivity emerge upon loosening of the quantum confinement in quantum dots?

Here, we report on the onset of real conductivity upon loosening the electronic quantum confinement in colloidal CdTe nanocrystals by increasing their size. The transition in conductivity behavior is probed by measuring the terahertz response of excitons that are optically excited in the quantum dots. The THz probe spectrum is broad and comprises the photon energies ranging from ~1 meV (~300 GHz) to about 10 meV. THz spectroscopy allows for contact-free conductivity measurements with very high (subpicosecond) time resolution.[7] We find evidence for the appearance of real-valued conductivity already for QD radii exceeding 5.3 nm. This is significantly smaller than the bulk exciton Bohr radius a_B of around 7 nm, which is defined through $a_B = \varepsilon_{nc}\hbar^2/\mu e^2$, where ε_{nc} is the dielectric constant (ε_{nc} = 10.6), $\hbar$ is the reduced Planck's constant, μ is the reduced exciton mass, and e is the electric charge. We show that the real conductivity does not arise from freely moving charges, but from polarons that are formed through resonant coupling between discrete hole transitions and optical phonons.

Methods. Colloidal CdTe nanocrystals with radii ranging from 3 to 8 nm were prepared by a modified SILAR procedure using smaller CdTe nanocrystals (3.5−5 nm diameter) as seeds (see Supporting Information for details).[8−10] The nanocrystal samples were characterized by optical spectroscopy (absorption and photoluminescence) and transmission electron microscopy (TEM). To remove excess surfactants and unreacted precursors, the samples for THz spectroscopy were purified by precipitation (see Supporting Information for details). Great care was taken to avoid the formation of rods for larger radii.

For the THz measurements, suspensions of nanocrystals in toluene were contained in fused silica cuvettes with an optical path length of 1 mm. The absorbance at the pump wavelength of 400 nm was determined with a spectrophotometer and kept below an optical density of 0.5. The corresponding nanocrystal concentrations were sufficiently low to avoid particle agglomeration, which could potentially disturb the results due to internanocrystal carrier transport. Furthermore, the excitation profile can be approximated to be constant over the whole cuvette length. The pump fluence was chosen sufficiently low such that the probability of biexciton generation was smaller than 5% for all measurements.

For the calculations of the electronic states and their complex polarizabilities we employed tight-binding (TB) calculations that are described in the Supporting Information.

The time-resolved THz time-domain spectroscopy setup is pumped by an amplified Ti:Sapphire laser operating at a repetition rate of 1 kHz, delivering pulses with a duration of 150 fs and an energy of 1 mJ at a wavelength of 800 nm. Ninety percent of the output energy is split off and frequency-doubled to a wavelength of 400 nm with a BBO crystal and used as the pump pulse (~5 μJ/cm^2). The remaining output is used to generate THz radiation via optical rectification in a 1 mm thick ZnTe crystal and to detect it in a second ZnTe crystal of similar size via electro-optic sampling.[11] The generated THz probe spectrum covers a broad frequency range spanning from 0.5 to 1.2 THz. One particular feature of the electro-optic detection method is that it works in the time-domain, that is, it directly records the electric field strength of the THz probe pulse. As opposed to most conventional spectrometers based on measuring intensity, this implies that not only changes in the absorption of the THz pulse can be detected, but also in the phase of the pulse. As a result, the THz frequency-dependent complex index of refraction (absorption coefficient and refractive index) of the investigated material can be deduced directly without having to resort to, for example, Kramers−Kronig relations. By modulating the pump beam with an optical chopper and recording the difference signal using a lock-in amplifier, we infer the pump-induced THz response, that is, the change in the complex index of refraction, which is directly related to the THz-frequency complex optical conductivity spectrum of the photoexcited excitons only.

Results. Figure 1 shows the photoluminescence spectra of a set of CdTe nanocrystal batches ranging in radius from 3.1 to

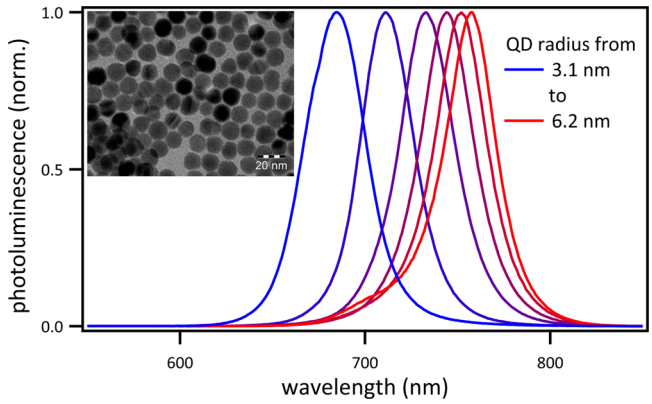

Figure 1. Photoluminescence spectra of CdTe nanocrystals with sizes ranging from 3.1 to 6.2 nm radius. The inset shows a TEM image of a batch of nanocrystals with mean radius of 7 nm.

6.2 nm. The redshift of the bandgap with increasing size is clearly visible, converging toward the bulk value of ~1.48 eV (840 nm). The inset shows a TEM image of nanocrystals with a mean radius of 7 nm. Additional TEM images are provided in the Supporting Information (Figures S1−S4). Analysis of the TEM results reveals that the nanocrystals are faceted but nearly spherical with a standard deviation in radius of about 7−10%.

We extract the exciton-induced change in the THz probe response of the nanocrystals suspension following the method described in ref 12 and express it in terms of the complex conductivity spectrum $\hat{\sigma}(\omega)$. Figure 2 shows two exemplary measured complex conductivities $\hat{\sigma}(\omega)$, determined ~10 ps after optical excitation, for batches of CdTe nanocrystals with a mean radius of 4.25 nm (Figure 2a) and 7.5 nm (Figure 2b). The real part of $\hat{\sigma}(\omega)$ is related to absorption, whereas the imaginary part indicates the phase response of the THz probe. The time evolution of the THz signal shows a reduction of 30−50% over a time scale of about 30 ps which has been attributed before to electron or hole trapping in surface states.[3] For sufficiently small quantum dots (Figure 2a), the real part of $\hat{\sigma}(\omega)$ is zero (no THz absorption), while significant real conductivity is observed for larger particles (Figure 2b). The appearance of real conductivity, that is, absorption, for the large particles indicates the existence of low-energy transitions that are resonant with the THz probe pulse.

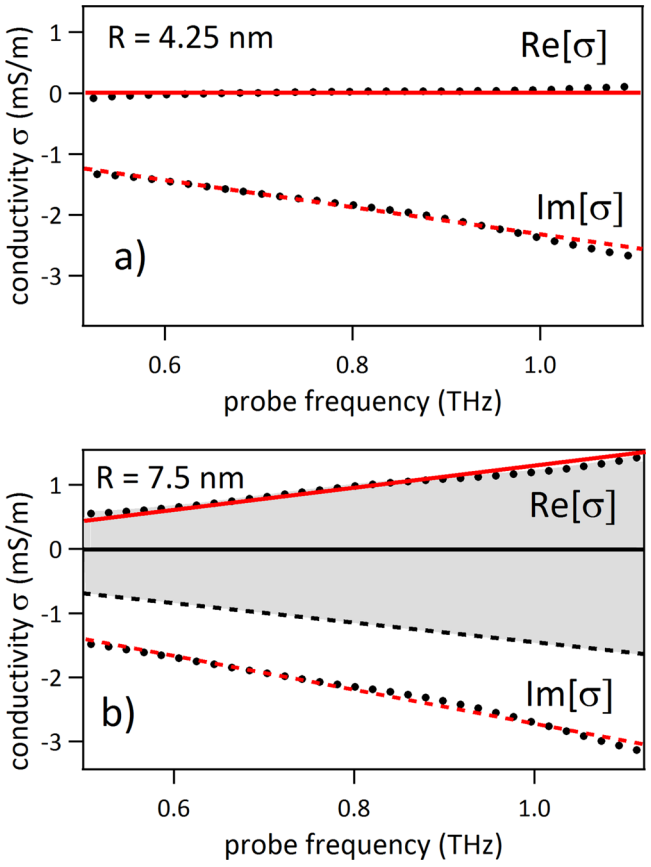

Figure 2. Exemplary THz conductivity spectra (black dots) for CdTe nanocrystal samples showing (a) no real conductivity and (b) finite real conductivity. Red solid (real part) and dashed (imaginary part) lines are the results of models for the exciton polarizability described in the text. The black lines in panel b show the electron contribution to the total exciton conductivity for this radius (solid, real part; dashed, imaginary part), and the gray-shaded area is the hole contribution.

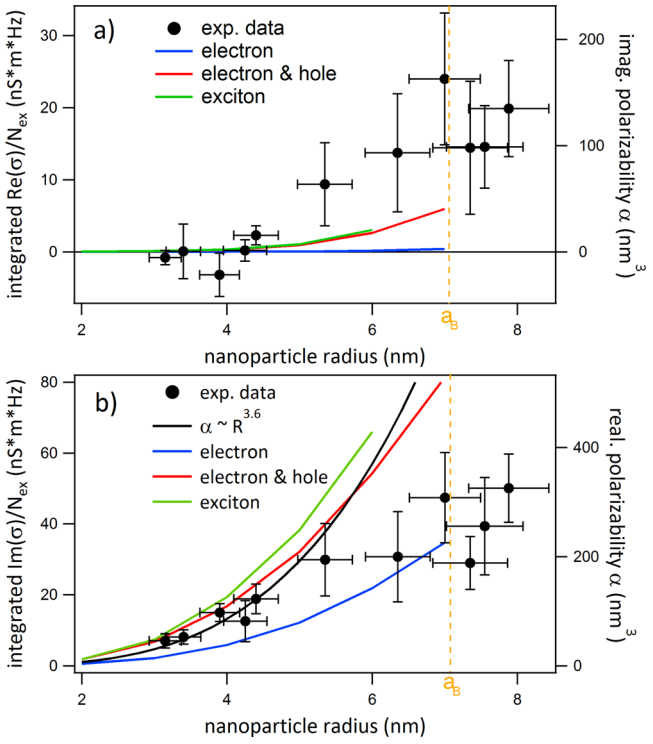

Figure 3. Spectrally integrated (a) real conductivity and (b) imaginary conductivity, divided by the excitation density N_{ex}. On the right axis: imaginary polarizability (a) and real polarizability (b). Black dots represent the experimental data. The vertical error bars were obtained from the standard deviation of the values extracted from various measurements on the same batch. The horizontal error bars are determined by the standard deviation of the particle size distribution, which is 7%. The black solid line in (b) sketches the $R^{3.6}$ dependence that was observed in previous publications for the exciton polarizability in the strong confinement regime. Colored solid lines are the results of the TB calculations (with broadening η = 5 meV): single electron in QD (blue), electron and hole without considering Coulomb interactions (red), electron and hole including Coulomb interactions (green). The yellow dashed line indicates the bulk exciton Bohr radius a_B = 7 nm.

Surprisingly, considering the Bohr radius of 7 nm, the largest radius for which we see no real conductivity is 4.4 nm. This observation is illustrated by Figure 3a, which shows a summary of the THz conductivities for all measured sizes. Plotted is the spectrally integrated real part of $\hat{\sigma}(\omega)$, divided by the sheet excitation density N_{ex}, which was determined experimentally from the absorption coefficient at the excitation wavelength of 400 nm.

Figure 3a reveals a clear change in the response at a nanocrystal radius of 5 nm. Below this radius no real conductivity is observed, while all larger nanocrystals show a finite real conductivity. We note that although the low measured signal amplitudes cause some scatter in the magnitude of the measured conductivities, significant real conductivity was always clearly observed for $R > 5$ nm, while it was never significantly larger than zero for $R \leq 4.4$ nm. Remarkably, the real conductivity sets in already for sizes significantly smaller than a_B. Apparently, a low-lying, quasi-continuous distribution of energy levels emerges for $R > 5$ nm.

For the smaller nanocrystal sizes, the conductivity is purely imaginary and negative, increasing linearly with frequency. This is due to the real polarizability $\mathrm{Re}(\hat{\alpha}) = \alpha'$ of the excitons within the QDs,[3] which is proportional to $\mathrm{Im}[\hat{\sigma}(\omega)] = \hat{\sigma}''(\omega)$, according to[13]

$$\hat{\sigma}''(\omega) = -\omega N_{ex} \frac{36\pi\varepsilon_S^2}{(\varepsilon_{nc} + 2\varepsilon_s)^2}\hat{\alpha}'$$

Similarly, $\mathrm{Re}[\hat{\sigma}(\omega)] = \hat{\sigma}'(\omega)$ is defined through

$$\hat{\sigma}'(\omega) = -\omega N_{ex} \frac{36\pi\varepsilon_S^2}{(\varepsilon_{nc} + 2\varepsilon_s)^2}\hat{\alpha}''$$

In both equations, ε_s is the dielectric constant of the solvent and ε_{nc} that of the nanocrystal. A fit to this model is shown by the red lines in Figure 2a, which includes the zero real conductivity. Figure 3b summarizes the extracted values for the spectrally integrated $\mathrm{Im}[\hat{\sigma}(\omega)]$, divided by the sheet excitation density N_{ex}. Previous measurements of the THz conductivity of carriers in nanoparticles[3,6,13,14] have mostly been performed for relatively small particles ($R < 3.5$ nm), for which generally zero real conductivity was observed (apart from ref 6), with the imaginary conductivity being determined by the exciton polarizability.[3,13,14]

Size-dependent polarizability measurements of carriers in semiconductor nanocrystals have previously revealed scaling laws of $\mathrm{Im}[\hat{\sigma}(\omega)] \sim \hat{\alpha}' \sim R^{3.6}$ for CdSe[3,13] and $\sim R^4$ for InAs.[14] Our data can be well described by $\mathrm{Im}[\hat{\sigma}(\omega)] \sim R^{3.6}$ scaling for

sizes up to 5 nm, as indicated by the black solid line, in analogy to CdSe, which is very similar to CdTe in terms of its band structure and electronic parameters, such as electron and hole effective mass. Above 5 nm, the data deviates from this trend, consistent with the appearance of the real conductivity shown in Figure 3a. For $R > 5$ nm, the imaginary conductivity is no longer solely defined by the polarizability of strongly confined carriers but also by the response of carriers experiencing weakened confinement.

Discussion. In the following, we discuss the observation of real conductivity for CdTe nanocrystals with radii larger than 5 nm. This behavior is directly linked to the loosening of electronic quantum confinement. The degree of electronic quantum confinement is generally roughly classified through the relation between the crystal size and the bulk exciton Bohr radius a_B, which yields 7 nm for CdTe. This criterion is however somewhat inappropriate in the strong and intermediate confinement regime of a material such as CdTe in which the effective masses of electrons and holes are very different.[5] In this size regime, it is more sensible to use the Bohr radii of separated electrons and holes, which are 5.6 and 1.4 nm, respectively. On the basis of these facts alone, one would expect that the influence of confinement effects on the electronic structure of holes vanishes for smaller sizes as compared to electrons. On the other hand, the emergence of real conductivity in our measurements coincides precisely with the electron Bohr radius.

The key question thus regards the origin of the real conductivity: are charge carriers in fact moving around freely inside the nanoparticles, in which case real conductivity would originate from the ohmic losses of the THz-field induced drift of the carrier? Are we probing the decreased level spacing between intraexcitonic states, that is, electronic transitions resonantly moving into the THz probe spectrum? Or is there yet a third effect?

In order to answer these questions, it is imperative to investigate the size-dependent electronic structure. Several distinct physical mechanisms play a role in the confinement, such as confinement effects on the single-particle (electron and hole) levels, electron–hole correlations, and dielectric polarization effects. The confinement regime investigated here is particularly intricate as, in contrast to the limiting cases of strong and weak confinement, approximations with respect to the confinement energy cannot be applied. In the strong confinement regime, electrons and holes are largely uncorrelated and their confinement can thus be treated separately with electron–hole correlations treated as a perturbation. On the other hand, in the weak confinement regime the excitonic contribution to the total confinement energy prevails.

We therefore performed TB calculations that fully include all confinement contributions for arbitrary QD size. They allow computing the electronic energy levels and, based on that, to calculate the complex exciton polarizability in the THz spectral range. The calculations reveal that the energy spacing between electron levels is always larger than those between hole levels. This is expected: due to its lower effective mass the electron wave function is more spread out than the hole wave function and thus confinement effects are stronger. Even for the $R = 6$ nm particles the transition energy between the electron ground state and the next-highest state still exceeds 60 meV. The electron transition energies are therefore too high to be relevant; hence only hole levels are considered for our discussion.

The calculated confinement energies of the hole levels, that is, their transition energies with respect to the ground state, are plotted for several sizes in Figure 4a. The lengths of the bars

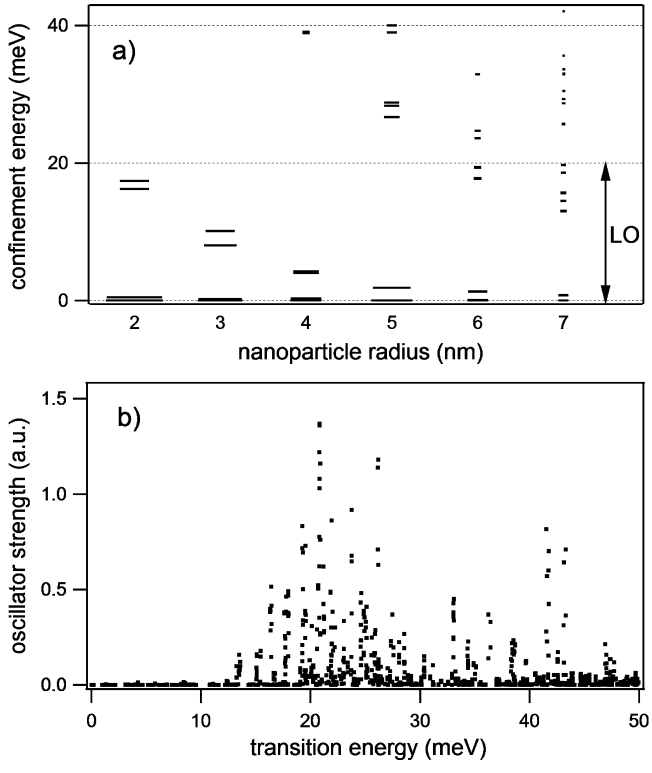

Figure 4. (a) Calculated hole energy states as a function of the CdTe nanocrystal radius. The length of the bar indicates the relative thermal occupation probability at room temperature and the double arrow the LO phonon energy of 21 meV; (b) oscillator strengths of all possible hole transitions, multiplied by the relative thermal occupation of the initial state, for nanocrystals of $R = 6$ nm.

indicate the relative thermal occupation at room temperature, where the sum of all probabilities equals one. It is evident that several energy levels are significantly populated and the energy spacing between them is still in the millielectronvolt range, also for the largest calculated size of 7 nm, and thus far from forming a continuum. The real conductivity increase is thus evidently not related to "true" conductivity as found in bulk semiconductors.

To explore whether the decreased level spacing between intraexcitonic states is responsible for resonant THz absorption, we calculated the size-dependent complex polarizabilities of all relevant electronic transitions. The polarizability at the transition energy $\hbar\omega$ is written as $-e^2F^2\Sigma_{n,m}[|\langle n\|m\rangle|^2(f_n - f_m)]/[\hbar\omega - (E_m - E_n) + i\eta]$ where $|n\rangle$ is a state of the system with energy E_n and thermal occupancy f_n, $\langle n\|m\rangle$ is the dipolar matrix element between states n and m, and F is the local-field factor. The factor η may account for the broadening of the transitions in particular due to coupling to phonons. We performed two types of calculations in which the states $|n\rangle$ are either single-particle TB states or excitonic states built from the TB states using a full configuration-interaction approach. The comparison between the two calculations sheds light on the effect of the electron–hole interaction on the polarizability.

Figure 3 displays the results of the calculations together with the experimental values. The colored solid lines show the calculated conductivities/polarizabilities for a single electron in

the QD (blue), an electron and hole without considering Coulomb interactions (red), and finally electron and hole including Coulomb interactions (green). The difference between the red and green curves is small. It is thus apparent that, as expected, the influence of Coulomb interactions is minor, particularly for smaller sizes. Electrons and holes contribute approximately equally to the real polarizability (see Figure 3b). The imaginary polarizability (real conductivity), as shown in Figure 3a, is however solely due to the hole, which starts to increase appreciably for sizes above 5 nm, which is in agreement with the experimental observation. It seems that our calculations can indeed qualitatively explain the onset of real conductivity as originating from the redshift of hole intraband transitions for increasing particle sizes whose resonances are approaching the THz probe window, a direct manifestation of weakening confinement. Quantitatively, however, the calculated results do not match the experimental values for $R > 5$ nm. For the larger QDs, the theory underestimates the real conductivity by a factor of 3, and overestimates the imaginary conductivity by about a factor two. The observed variance points to a type of light-matter coupling mechanism that is not accounted for in our calculations.

The discrepancy may be traced to the fact that the complex polarizability as computed here only considers optical transitions between electronic states but the effects resulting from carrier-phonon coupling are only described through a simple, phenomenological broadening η of the transition lines. The calculations used $\eta = 5$ meV; further broadening did not appreciably alter the polarizabilities. The real conductivity remains much smaller than the measured value irrespective of η.

A plausible and likely scenario that explains the present deviation, which is not accounted for in the TB calculations, is that at $R > 5$ nm electronic transitions become resonant with optical phonon modes and the resulting coupling creates mixed polaron states. In that case, one can expect additional transitions to emerge, for the polaron allows coupling of THz probe photons to optical phonon modes.[15] To illustrate this scenario, it is instructive to look again at the computed size-dependent electronic energy levels of Figure 4a.

The lowest hole states are composed of multiplets with splittings in the sub-to-few-millielectronvolt range for the largest sizes. For symmetry reasons, the oscillator strength for transitions between these multiplets is practically zero. This is shown in Figure 4b which plots the oscillator strengths of all possible hole transitions, multiplied by the relative thermal occupation of the initial state, for nanocrystals of $R = 6$ nm. The oscillator strength is zero for all transitions below 10 meV. The longitudinal optical (LO) phonon energy in CdTe is 21 meV and is largely unaffected by confinement effects.[16] For radii approaching 6 nm the energy between the two lowest states and the next-higher ones falls below 20 meV, which matches the LO phonon frequency (indicated by the arrow labeled LO in Figure 4 a). Other transitions become resonant with the LO phonon frequency, too. In fact, a summation over the oscillator strengths for all transitions of thermally populated hole states shows a drastic enhancement of the total oscillator strength around 20 meV when going from 5 nm (where the oscillator strength at 20 meV is zero, and coupling between hole−hole transitions and LO phonons thus impossible) to 6 nm size (where the hole intraband transition energies have approached the LO phonon energy). The latter situation is shown in Figure 4b. It has been shown before that such a situation in which electronic transitions in quantum dots become resonant with LO phonon modes, can lead to the formation of mixed carrier-phonon, that is, polaron, states.[15] The coupling through Fröhlich interaction can be described by an entangled two-level system with wave function $|\Psi_i\rangle$ which is comprised of the uncoupled excited hole state $|h_{i,\mathrm{exc}}\rangle|0_{\mathrm{LO}}\rangle$ and the hole ground state, which is coupled to the one-LO-phonon mode $|h_{i,\mathrm{g}}\rangle|1_{\mathrm{LO}}\rangle$[15]

$$|\Psi_i\rangle = x|h_{i,\mathrm{exc}}\rangle|0_{\mathrm{LO}}\rangle \pm \sqrt{1-x^2}\,|h_{i,\mathrm{g}}\rangle|1_{\mathrm{LO}}\rangle$$

At room temperature, a large number of polaron states are populated (hence the subscript i in $|\Psi_i\rangle$) with presumably each of them possessing different coupling strengths to the probe light. The polaron state essentially permits coupling of the THz probe light to optical phonons by exciting the phonon part of the polaron wave function $|\Psi_i\rangle$, which would give rise to new absorption features associated with the phonon excitation when the polaron eventually relaxes via its LO phonon component through anharmonic coupling into a continuum of multi-phonon states. The coupling between $|h_{i,\mathrm{exc}}\rangle|0_{\mathrm{LO}}\rangle$ and $|h_{i,\mathrm{g}}\rangle|1_{\mathrm{LO}}\rangle$ strongly varies with size (approx. $\sim 1/R$), but the maximum entanglement ($x^2 \approx 1/2$) is obtained when the electronic transition is in resonance with the LO phonon energy. In the case of CdTe nanocrystals, strong polaronic effects are thus maximum for radii in the range of 6−8 nm as shown by the TB calculations. In the range of 6−8 nm, the coupling strength is large, but only weakly dependent on size, explaining why the real conductivity is rather constant in this range. The smallest size for which we see real conductivity is 5.3 nm, which is slightly below the anticipated polaronic size range. This deviation can be attributed to the size dispersion of the nanocrystals (~0.5 nm) and uncertainties in the TB calculations of the energy levels, which put an additional error margin on the energy range.

In order to isolate the anticipated hole polaron THz response from the measured THz spectra, we subtract the electron contribution. The electron contributes only to the imaginary part of the measured conductivities through its polarizability. Figure 3 shows that the electron contributes to approximately half to the total imaginary conductivity. The resulting hole response can be described well by an overdamped Lorentzian oscillator with a center frequency of (18.5 ± 5.2) meV and width of (38.2 ± 10.6) meV. A fit to this model is shown in Figure 2b, where the red lines depict the total polarizability, the black lines depict the electron contribution, and the gray-shaded area is the hole contribution. The errors to the values are derived from the standard deviation of the fitted parameters extracted from approximately 50 measurements. Within experimental error, the inferred center frequency of 18.5 meV is indistinguishable from the LO phonon energy of 21 meV, corroborating our picture that polaron states are the main source of the emerging real conductivities at R > 5 nm.

Thus, a transition takes place from confined carriers to polaron states with increasing QD size, even below the Bohr radius. The occurrence of polaron states leads to a drastically different optical response, which is relevant for potential applications that exploit intraband transitions in nanocrystals for optoelectronic purposes such as recently proposed low-threshold lasers.[17,18] The awareness of this effect can also be important for the study of the THz conductivity response of coupled nanocrystal films.

Conclusions. In conclusion, we have investigated the THz response of photogenerated excitons in CdTe nanocrystals of

radius between 3 and 8 nm, ranging in size from the strong to the weak quantum confinement regime. For nanocrystal radii below 5 nm we only measure an imaginary conductivity originating from the polarizability of strongly confined excitons, which is in agreement with previous publications. Above 5 nm, we observe the onset of real conductivity, which we attribute to THz transitions induced by confinement-induced strong coupling between low-lying hole states and LO phonons, giving rise to optically highly active polaron states.

■ ASSOCIATED CONTENT

Supporting Information

Methods, characterization, tight-binding calculations, and Figures S1–S4. This material is available free of charge via the Internet at http://pubs.acs.org.

■ AUTHOR INFORMATION

Corresponding Author

*E-mail: bonn@mpip-mainz.mpg.de.

Notes

The authors declare no competing financial interest.

■ ACKNOWLEDGMENTS

The authors would like to thank Tony Heinz for inspiring discussions. The work is part of the research program of the Foundation for Fundamental Research on Matter, which is financially supported by the Dutch organization for Scientific Research (NWO). This work has been financially supported by the European Union Marie Curie Program (MEST-CT-2005-021000) and by the EU Seventh Framework Program (EU-FP7 ITN Herodot).

■ REFERENCES

(1) Smyder, J. A.; Krauss, T. D. Coming attractions for semiconductor quantum dots. *Mater. Today* **2011**, *14* (9), 382–387.

(2) Efros, A. L.; Efros, A. L. Interband light absorption in a semiconductor sphere. *Semiconductors* **1982**, *16*, 1209–1214.

(3) Wang, F.; et al. Exciton polarizability in semiconductor nanocrystals. *Nat. Mater.* **2006**, *5* (11), 861–864.

(4) Empedocles, S. A.; Bawendi, M. G. Quantum-confined stark effect in single CdSe nanocrystallite quantum dots. *Science* **1997**, *278* (5346), 2114–2117.

(5) Efros, A. L.; Rosen, M. The electronic structure of semiconductor nanocrystals. *Annu. Rev. Mater. Sci.* **2000**, *30*, 475–521.

(6) Beard, M. C.; Turner, G. M.; Schmuttenmaer, C. A. Size-Dependent Photoconductivity in CdSe Nanoparticles As Measured by Time-Resolved Terahertz Spectroscopy. *Nano Lett.* **2002**, *2* (9), 983–987.

(7) Ulbricht, R.; et al. Carrier dynamics in semiconductors studied with time-resolved terahertz spectroscopy. *Rev. Mod. Phys.* **2011**, *83* (2), 543.

(8) Donega, C.d.M.; Koole, R. Size Dependence of the Spontaneous Emission Rate and Absorption Cross Section of CdSe and CdTe Quantum Dots. *J. Phys. Chem. C* **2009**, *113* (16), 6511–6520.

(9) Wuister, S. F.; Donega, C. D. M.; Meijerink, A. Luminescence Temperature Antiquenching of Water-Soluble CdTe Quantum Dots: Role of the Solvent. *J. Am. Chem. Soc.* **2004**, *126* (33), 10397–10402.

(10) Yu, W. W.; Wang, Y. A.; Peng, X. G. Formation and Stability of Size-, Shape-, and Structure-Controlled CdTe Nanocrystals: Ligand Effects on Monomers and Nanocrystals. *Chem. Mater.* **2003**, *15* (22), 4300–4308.

(11) Nahata, A.; et al. Coherent detection of freely propagating terahertz radiation by electro-optic sampling. *Appl. Phys. Lett.* **1996**, *68* (2), 150–152.

(12) Hendry, E.; et al. Interchain effects in the ultrafast photophysics of a semiconducting polymer: THz time-domain spectroscopy of thin films and isolated chains in solution. *Phys. Rev. B* **2005**, *71* (12), 125201.

(13) Dakovski, G. L.; et al. Terahertz Electric Polarizability of Excitons in PbSe and CdSe Quantum Dots. *J. Phys. Chem. C* **2007**, *111* (16), 5904–5908.

(14) Pijpers, J. J. H.; et al. (Multi)Exciton Dynamics and Exciton Polarizability in Colloidal InAs Quantum Dots. *J. Phys. Chem. C* **2010**, *114* (14), 6318–6324.

(15) Grange, T.; Ferreira, R.; Bastard, G. Polaron relaxation in self-assembled quantum dots: Breakdown of the semiclassical model. *Phys. Rev. B* **2007**, *76* (24), 241304.

(16) Dimitrov, S. D.; et al. Femtosecond Probing of Optical Phonon Dynamics in Quantum-Confined CdTe Nanocrystals. *J. Phys. Chem. C* **2009**, *113* (10), 4198–4201.

(17) Hsu, C. F.; et al. Intersubband quantum-box semiconductor lasers. *IEEE J. Selected Topics Quantum Electronics* **2000**, *6* (3), 491–503.

(18) Prodanovic, N., et al., Relationship between electron-LO phonon and electron-light interaction in quantum dots. *Phys. Rev. B*, **2012**. *85*(19).